Biomechanical Evaluation of Temporomandibular Joint Implants Under Complete Mastication Cycle

Rajdeep Ghosh[1,2,3], Girish Chandra[1], Vivek Verma[1], Kamalpreet Kaur[4], Ajoy Roychoudhury[4], Sudipto Mukherjee[1], Anoop Chawla[1], Kaushik Mukherjee[1,*]

[1]*Department of Mechanical Engineering, Indian Institute of Technology Delhi, New Delhi 110 016, Delhi, India*

[2]*Department of Mechanical Engineering, University of Sheffield, Sheffield S1 3JD, United Kingdom*

[3]*INSIGNEO Institute for in silico Medicine, University of Sheffield, Sheffield S1 3JD, United Kingdom*

[4]*Department of Oral & Maxillofacial Surgery CDER, All India Institute of Medical Sciences Delhi, New Delhi 110029, Delhi, India*

*Corresponding author:

Dr. Kaushik Mukherjee

Department of Mechanical Engineering

Indian Institute of Technology Delhi

New Delhi, 110 016

Tel: +91 – (0) 3612 – 583211

Email: kumukherjee@mech.iitd.ac.in

Keywords: *Temporomandibular joint (TMJ) implant; Mandible; Mastication cycle; FE analysis*

Submitted to: Computer Methods and Programs in Biomedicine
Word Count: Abstract 210; Manuscript 3472
Number of Tables: 2; Number of Figures: 5

Abstract

To ensure the long-term success of temporomandibular joint (TMJ) implants, it is imperative to understand their biomechanical performances under the mastication cycle. In the present study, patient-specific QCT-based finite element models of a human mandible were developed. The left TMJ was virtually replaced by stock implants (narrow and standard). A complete mastication cycle involving six clenching tasks was simulated. A comparative biomechanical assessment between the intact and the implanted mandibles was performed based on maximum principal stress and strain distributions on the mandible. As compared to contralateral occlusion, ipsilateral clenching resulted in higher strains in the mandible. However, contralateral occlusion produced a larger von Mises stress on the implant than ipsilateral occlusion. Furthermore, intercuspal (ICP) biting was found to have produced the highest strain (1750-1880 $\mu\varepsilon$) and stress (16.02-16.54 MPa) in the mandible. As compared to immediate post-operative non-osseointegrated (NOI) conditions, an overall reduction of stress (narrow TMJ: 0.14 MPa; standard TMJ: 0.12 MPa) and strain (narrow TMJ: 30 $\mu\varepsilon$; standard TMJ: 20 $\mu\varepsilon$) was observed in post-operative osseointegrated (OI) phase. Although stresses and strains in mandible and implants are reduced in OI condition, standard TMJ produced higher stresses in cortical bone compared to narrow TMJ during NOI conditions, which suggests the possible preference of narrow TMJ over standard ones.

1. Introduction

A wide range of disorders, primarily intra-articular pathologies, and trauma [1–3], can affect the temporomandibular joint (TMJ), causing clinical symptoms such as pain, restricted joint movement, malocclusion, and functional difficulty during deglutition and speech [4,5]. TMJ replacement with an alloplastic joint may be required for patients who do not respond well to conservative and non-surgical treatment [1]. Despite the short-term successes associated with the use of TMJ implants, the long-term implications of these commercially available stock TMJ implants are still not clear to the scientific community and clinicians [6–9].

The patient-specific TMJ Concepts system (Stryker, Ventura, CA, USA) and the stock Zimmer Biomet Microfixation systems (Jacksonville, FL, USA) are the two primary US-FDA-approved TMJ replacement systems now available globally. Patient-specific implants are designed to match the anatomical periphery of the host bone for better stability and ease of implantation [10,11]. However, the use of patient-specific implants is not as prevalent as the stock ones due to higher cost and longer delivery times [12]. Biomet Microfixation system® designed stock mandibular prosthesis comes in two shapes viz. standard (45 mm, 50 mm and 55 mm) and narrow (45 mm and 50mm) with varying sizes depending on the length of the mandibular body. The choice between standard and narrow implants depends on factors such as patient anatomy, surgical requirements, and the extent of joint reconstruction needed. A report from a recent meta-analysis by Zou et al.[13] revealed comparable outcomes between stock and patient-specific prostheses in terms of reduced pain score and improvement in function score, diet score, and maximum incisal opening. However, these implants (especially stock implants) are vulnerable to long-term failure risks primarily owing to implant design, poor material selection, improper surgical techniques etc.[7,8]. Therefore, further research is needed to achieve a longer life span for existing TMJ implants [6,13].

The human mandible experiences different physiological loads throughout its lifetime. Although there have been several *in silico* studies on biomechanical assessment of healthy [14–20] and reconstructed human mandibles [21–29], only a few studies have investigated reconstructed human mandibles with TMJ implants [24,26,27]. Notable among them is the study by Pinheiro et al. [26] which reported the strain and deformation across the human mandible implanted with a patient-specific TMJ implant under three clenching tasks. Their study considered a frictionless interface between the bone-implant and condyle-fibrocartilage. A frictionless interface typically indicates an extremely smooth interface which offers no resistance against relative movement. While this might be true for the condyle-fibrocartilage joint, the bone-implant interfaces are typically modelled as frictional [30] or bonded [31]. Additionally, such simplified bone-implant interface modelling would also influence the stress-strain behaviour across the mandible and TMJ implant.

To the authors' knowledge, none of the studies reported the influence of different stock TMJ implants on load transfer across the human mandible under both unilateral and bilateral clenching activities. The present study is thus aimed at gaining an insight into the biomechanical performance of two stock TMJ implants (standard and narrow types by Zimmer Biomet Microfixation systems®) under unilateral and bilateral clenching tasks representing a complete mastication cycle. In addition, the influences of bone-implant interface conditions, representing an osseointegrated and non-osseointegrated conditions, on stresses and strains in implanted mandible were also investigated.

2. Materials and Methods

Quantitative computed tomography (QCT)- dataset (512 x 512 pixels; voxel size of 0.439 × 0.439 × 0.75 mm^3) of an anonymized 20-year-old healthy male subject was obtained to develop the model of the intact mandible. A 3-D surface model of the intact mandible was reconstructed in Materialise Mimics v25.0 (Materialise Inc., Leuven, Belgium). Finite

element (FE) mesh was generated in Hypermesh v2022 (Altair Engineering Inc., Troy, MI, USA), whereas FE simulation and further post-processing were performed in Ansys APDL v2022 R2 (ANSYS Inc., Canonsburg, PA, USA).

2.1 Development of Intact FE model

The human mandible (Figure 1) has the following major components: cortical, cancellous, periodontal ligament (PDL), teeth, articular fibrocartilage, and temporal bone (represented by cubic block). Due to considerable influence of PDL layer on stress-strain distribution in human mandible [16], it was decided to model the PDL (~ 0.3 mm thickness) and this was achieved by offsetting the interface between the cancellous bone and the teeth. PDL was further divided into three subcomponents along the root length: coronal, middle, and apical thirds. All components were meshed with 10-noded tetrahedral elements (with edge lengths from 0.3 mm to 2 mm) by fulfilling appropriate mesh quality parameters such as aspect ratio (<5), Jacobian ratio (>1), etc. A mesh convergence study was performed with an ascending number of elements from coarse (305,774 elements), to medium (3,403,988 elements), to fine (7,054,373 elements) element sizes on the intact model. However, difference in maximum principal stress in the mandible was predicted to be 5% between coarse and medium meshed models, while 0.4% between the medium and fine meshes. Therefore, the medium meshed model with element sizes ranging between 0.5 mm to 1.5 mm (3,403,988 elements) was chosen as the optimum FE model for further investigation in this study. -

2.2 Development of Implanted FE models

The 3D models of the mandibular components of TMJ implants (Figure 2 - a & b) were developed from the micro-CT images (Xtreme CT II, Scanco Medical AG, Switzerland, with scanning parameters: 491 x 256 pixels; isometric voxel size of 60 μm) of narrow and standard stock implants of size 45 mm (Zimmer Biomet Microfixation system, Jacksonville, FL, USA). Based on Biomet mandibular screws [32], bi-cortical screws were modelled as

simplified cylinders (Φ2.7 mm) with lengths ranging from 8 – 12 mm. The models of the intact mandible and TMJ implant were imported into Rhinoceros® software (Rhinoceros V7.0, Robert McNeel & Associates, Seattle, USA) for osteotomy and virtual implantation based on clinical recommendations. A medium mesh (edge length between 0.5 – 1.5 mm) was used for TMJ implants (Figure 2 - c & d).

2.3 Material Properties

In this study, linear elastic orthotropic material properties were assigned to different regions of mandible. Cortical bone was modelled as a region-specific orthotropic material [14]. Cancellous bone, however, was modelled as homogeneous orthotropic material [14]. All other components such as teeth, PDL, fibrocartilage and implant were modelled as linear elastic isotropic material [21,28] Temporal bone was modelled as a rigid body [21]. Table 1 shows the material properties used in this study for different components. For the implanted mandible, the mandibular component and the screws were assumed to be made of medical grade Ti-6Al-4V extra-low interstitial (ELI).

2.4 Loading and Boundary Conditions

The following six biting tasks (Table 2) were considered in this study: incisal (INC), intercuspal (ICP), right molar (RMOL), left molar (LMOL), right group (RGF), and left group (LGF) biting. Muscle activity of seven muscles (Figure 2-e) [33] namely, two masseter (SM/DM), two pterygoid (MP/LP), and three temporalis muscles (AT/MT/PT) were considered in this study. However, the influence of lateral pterygoid was neglected on the implanted side of the implanted model as total joint replacement requires excision of condyle where the lateral pterygoid muscle is attached. In addition, the present study hypothesized that all the muscles reattached successfully post-implantation. The top surface of temporal bone blocks was fixed in all directions [14,33]. The bite points corresponding to each biting tasks were constrained in Z-direction [26]. To investigate the influence of bone-implant

interface conditions on stress-strain distribution across the bone and implant, both osseointegrated (OI) and non-osseointegrated (NOI) bone-implant interface conditions have been considered here. To model the osseointegrated (OI) condition, the interface between mandibular component and cortical bone was bonded whereas a frictional interface between mandibular component and cortical bone was considered to mimic the non-osseointegrated (NOI) condition. Furthermore, the frictional contact between articular fibrocartilage and mandibular condyle was defined in the intact and implanted mandibles. Frictional contact was also considered between the head of the mandibular component and temporal bone block in the implanted mandible. All the other contact pairs were defined as bonded. An 'Augmented Lagrangian Algorithm' was defined for all surface-to-surface frictional contact pairs ($\mu = 0.3$).

2.5 Interpretation of Results

Mandible exhibits a sandwich structure wherein the cortical bone bears most of the clenching load. Cortical bone being brittle in nature, prior studies considered maximum principal strains as failure criterion [34,35]. Therefore, in the current study, maximum principal strains and stresses in the mandible were considered for biomechanical comparisons between the intact and implanted mandibles. To exclude singular values, owing to constrained regions in the FE models in both intact and implanted mandibles, 99th percentile values of principal stresses and strains of cortical bone were considered for comparison. Conversely, implants being made of Ti6Al4V which exhibits ductile material behaviour, von Mises stress was considered for investigating the load transfer through narrow and standard TMJ implants under complete mastication cycle.

2.6 Verification of Intact FE model

Since the CT-scan dataset was derived from a living subject, the FE model developed in the present study could not be directly validated by a one-to-one experiment. However, a

qualitative and quantitative verification of the FE model was performed by comparing the results with those from earlier studies [14,18,26,36]. The present study observed a maximum principal stress of 11.87 MPa around the biting surfaces of the right molar teeth which corroborates a similar finding (15 MPa to 25 MPa) reported in a previous study by Korioth et al. [14] during a right molar clenching. The present study observed high maximum principal strains [700-1750 με] in all the load cases in healthy mandible. The magnitude of the principal strain observed near the anterior ramus surface of the mandible during the RMOL case in the present study was 1250 με, which closely matches the strain (1260 με) observed earlier [26]. Similar to the study by [36] high tensile strains below the mandibular notch and anterior surface of the condylar neck were also observed here (Fig 3). Gröning et al. [18] reported highest principal strains around the *pars alveolaris* below the molars, oblique line, *basis mandibulae*, and posterior ramus inferior to condyle during INC, ICP and molar bites (RMOL/LMOL). Similar strain distributions were observed in the present study for INC, ICP, and molar bites. The quantitative difference in results in maximum principal stresses and strains between this study and the erstwhile works [14,26] might be attributed to the difference in bone morphology, choice of bone material properties, and in muscle attachment sites. Notwithstanding subtle differences, the results from the present study provide confidence in the developed FE models.

3. Results

The principal stress and strain on the intact and implanted mandibles along with von Mises stress in the TMJ implants (mandibular component and screws) during immediate post-operative non-osseointegrated (NOI) condition are discussed first (section 3.1 and 3.2). Thereafter, influence of osseointegration on stresses and strains has been investigated by comparing the non-osseointegrated results with those of the osseointegrated (OI) models (section 3.3).

3.1 Maximum Principal Stress and Strain Distribution in Intact and Implanted Mandibles

Figure 3 shows the maximum principal stress distribution around intact and implanted mandibles under six different biting tasks representing a complete mastication cycle. The maximum tensile stress in the intact mandible ranges between 5.85 MPa (LGF) and 16.02 MPa (ICP). Higher stress regions were observed along the oblique line, anterior ramus, and across lateral alveolar regions in discrete patches for the molar (RMOL) and intercuspal (ICP) occlusion. For the rest of the load cases (INC/LGF/RGF), higher stresses were observed mostly near the molars in the alveolar region and around the medial mandibular notch. Minor difference in stress magnitude (narrow TMJ: 1.02 MPa; standard TMJ: 0.75 MPa) was observed between the intact and the implanted mandibles. However, marginally higher stress (maximum difference of 0.32 MPa) was observed in mandible with standard TMJ implant as compared to the one with narrow TMJ implant. Moreover, an overall increase in stress was observed in case of contralateral clenching (RMOL and RGF) as compared to ipsilateral ones (LMOL and LGF).

Figure 4 shows the distribution of maximum principal strain in the intact and reconstructed mandibles in a mastication cycle. The strain in the intact mandible over the full mastication cycle ranges from 700 με to 1750 με. Higher strains (1150 με to 1750 με) were observed during molar biting (RMOL and LMOL) and ICP cases across the ramus primarily around the lower condyles, coronoid process, oblique line and lateral surfaces of alveolar and body. However, INC and group function tasks (RGF/LGF) resulted in lower strains (700 με to 730 με) mostly around medial surfaces of mandibular notch and alveolar region on lateral sides. The ICP clenching caused the highest tensile strain (1750 με to 1880 με) among all the load cases.

An overall reduction in the magnitude of peak strain was observed in implanted mandibles (narrow TMJ: 80 με; standard TMJ: 120 με) as compared to those in intact mandible. However, higher strains (up to 80%) were observed around the screw holes in the implanted ones as compared to the intact mandible. Unlike intact mandibles, maximum principal strains in implanted mandibles increased under ipsilateral clenching (up to 14.75%) than contralateral ones (Figure 4). However, an opposite trend was observed for ipsilateral gonial angle region wherein strains under ipsilateral loading was higher (by 11.9%) than those under contralateral loading.

3.2 Stresses in Implants

Figure 5 shows the von Mises stress distribution across the implants and screws under different biting conditions. Among all the loading conditions, peak von Mises stress in the mandibular component of ramus standard TMJ was the highest (150.76 MPa) under RMOL, whereas the lowest (57.53 MPa) under LMOL. In comparison, for narrow TMJ implant, the highest (131.97 MPa) and lowest (87.21 MPa) von Mises stresses in mandibular component were observed under RGF and LGF, respectively. In general, ipsilateral clenching (LMOL/LGF) resulted in reduced von Mises stresses (standard TMJ: 93.23 MPa; narrow TMJ: 44.76 MPa) in mandibular component as compared to contralateral clenching (RMOL/RGF). Regions near the base of the mandibular component experienced negligible stresses (≤5MPa in standard TMJ implants (Fig. 5). Peak von Mises stresses in the screws were minimum during LMOL (narrow TMJ: 49.90 MPa; standard TMJ: 52.25 MPa). In comparison, higher stresses in the screws were observed during INC (narrow TMJ: 114.57 MPa; standard TMJ: 128.1 MPa) and RGF (narrow TMJ: 108.55 MPa; standard TMJ: 129.49 MPa). Additionally, stresses in the screws were higher in standard TMJ implant as compared to narrow TMJ implant during immediate post-operative non-osseointegrated condition. Overall stress patterns in the screws under all the loading conditions were similar.

3.3 Influence of osseointegration on stresses and strains in implanted mandible

The present study investigated both immediate post-operative non-osseointegrated (NOI) and long-term post-operative osseointegrated (OI) conditions. The interfacial conditions were found to influence the stresses (Figure 3) and strains (Figure 4) in the mandible and implant. Overall reduction in stress (narrow TMJ: 0.14 MPa; standard TMJ: 0.12 MPa) and strains (narrow TMJ: 30 $\mu\varepsilon$; standard TMJ: 20 $\mu\varepsilon$) were observed due to osseointegration. However, in mandibular component, an increase in stress was observed under contralateral loading as compared to ipsilateral loading for both NOI and OI conditions. During NOI condition, von Mises stresses in mandibular component during LMOL (narrow TMJ: 92.65 MPa; standard TMJ: 57.53 MPa) and LGF (narrow TMJ: 87.21 MPa; standard TMJ: 86.17 MPa) were found to be much lower than those during RMOL (narrow TMJ: 131.20 MPa; standard TMJ: 150.76 MPa) and RGF (narrow TMJ: 131.97 MPa; standard TMJ: 110.77 MPa) loading conditions. A similar observation is noted for OI condition as well (Figure 5). Although there is an overall reduction in stress in the standard TMJ implants as compared to the narrow ones in the OI condition, stresses in the implants during both OI and NOI conditions were much below the yield limit of the implant material (~955 MPa) [37]. In addition, reduction in stresses (up to 5.24 MPa) on the screws were also found in the standard TMJ implant compared to that on the narrow ones in the OI condition. Conversely, stresses increased (up to 22.87 MPa) in the standard TMJ implants in the NOI conditions.

4. Discussion

The present study is aimed to assess biomechanical performance of two widely used stock mandibular TMJ implants (standard and narrow) under the complete mastication cycle including both unilateral and bilateral clenching activities. In addition, influences of osseointegration on the stresses and strains in mandible and TMJ implants have also been

investigated.

Minor difference in stress magnitude across the mandible between the intact and implanted mandibles was observed in this study. Although mandibles implanted with standard TMJ implants resulted in slightly higher stresses (0.05-0.34 MPa) in cortical bone, the overall spatial distribution of cortical bone stresses were similar in all the cases. Higher cortical bone strains were, however, observed around the screw holes. This might cause fibrous tissue formation at the bone-implant interface [38], [39] in the long term. Similar observation was also reported in earlier clinical study [40]. Sugiura et al.[41] reported a threshold compressive strain (3600 $\mu\varepsilon$) for inducing bone resorption in human mandibles. The peak strain reported in the present study in implanted mandibles with both implants is much below the critical threshold limit for bone resorption which ensures the suitability of these implants in the present scenario. Higher strains (up to 14.75%) on implanted bone were observed under ipsilateral loading as compared to the contralateral ones, which is in contrast with the observations for intact bone. A similar trend of strains under ipsilateral and contralateral loading was also reported earlier [26].

Bone-implant interface condition was found to influence load transfer through mandibular component. An overall reduction in stresses were observed due to osseointegration similar to a recent study on dental implants [42]. During the initial NOI condition, screws act as mechanism to transfer loads from the mandible to the mandibular component and vice versa. On the contrary, during the OI condition, the entire bone-implant interface becomes osseointegrated and therefore, load-sharing happens through a larger interfacial area. Hence, a reduction in peak von Mises stress in implant and screws due to osseointegration is observed. Although implant and screw stresses remained within the corresponding yield limit during both nonosseointegrated and osseointegrated (OI)

conditions, during nonosseointegrated condition, screw stresses were higher in standard TMJ implant than those of the narrow TMJ implant. Therefore, based on this study, although both the stock implants were found to be safe, narrow TMJ is preferred over standard TMJ for joint replacement.

There were certain limitations of the present study. Even though the bone is heterogeneous anisotropic, the material property of cortical and cancellous bone was considered as a region-specific orthotropic material in the current work[14]. Modelling screws as cylindrical entities, while neglecting its threads, is another limitation of the present study. However, detailed thread modelling is primarily necessary when the focus is on understanding the stress-strain distribution at the screw thread interface [43,44] and, therefore, this assumption will not influence the overall prediction of this current study. In addition, inter-patient anatomical and muscle force variations of the human mandible were neglected in this study. Despite these limitations, this study on stock TMJ implants provide a thorough understanding on the performance of different stock implants under clenching loads and is expected to assist clinicians to choose a proper design of patient-specific TMJ implant.

5. Conclusion

To summarize, the present study investigated the biomechanics of narrow and standard TMJ implants on a patient-specific human mandible under different biting tasks representing a complete mastication cycle. Ipsilateral clenching resulted in higher strains in implant as compared to contralateral clenching. Overall, stresses and strains in the cortical bone, TMJ implants and screws were well below the corresponding failure limits for all the models. While osseointegration reduced stresses and strains in cortical bone for both the stock implants, a standard TMJ implant induced higher stress in cortical bone and higher strains in screws as compared to narrow TMJ implant during immediate post-operative non-

osseointegrated condition. Therefore, this study suggests that although both standard and narrow TMJ implants were found to be safe for joint replacements, narrow TMJ implant should perhaps be preferred over the standard ones.

CRediT authorship contribution statement

Rajdeep Ghosh: Conceptualization, Data Curation, Formal Analysis, Investigation, Methodology, Software, Validation, Visualization, Writing – original draft, Writing – review & editing. **Girish Chandra:** Conceptualization, Data Curation, Formal Analysis, Methodology, Visualization, Writing – review & editing. **Vivek Verma:** Data Curation, Visualization, Writing – review & editing. **Kamalpreet Kaur:** Writing – review & editing. **Ajoy Roychoudhury:** Funding acquisition, Project Administration, Resources, Supervision. **Sudipto Mukherjee:** Conceptualization, Funding acquisition, Methodology, Project Administration, Resources, Supervision, Writing – review & editing. **Anoop Chawla:** Conceptualization, Funding acquisition, Methodology, Project Administration, Resources, Supervision, Writing – review & editing. **Kaushik Mukherjee:** Conceptualization, Funding acquisition, Methodology, Project Administration, Resources, Supervision, Writing – review & editing.

Declaration of competing interest

There are no possible conflicts of interest for the authors in terms of funding support, research, authorship, or publishing of this paper.

Acknowledgments

The study was supported by the Indo–German Science & Technology Centre (IGSTC), under grant no. IGSTC/Call 2020/add-bite/48/2021-22/260.

References:

[1] A. Roychoudhury, P. Yadav, O. Bhutia, R. Mane, R. Yadav, D. Goswami, A. Jose,

Alloplastic total joint replacement in management of temporomandibular joint ankylosis, J. Oral Biol. Craniofacial Res. 11 (2021) 457–465. https://doi.org/10.1016/j.jobcr.2021.05.006.

[2] K. Bhatt, A. Roychoudhury, O. Bhutia, R.M. Pandey, Functional outcomes of gap and interposition arthroplasty in the treatment of temporomandibular joint ankylosis, J. Oral Maxillofac. Surg. 72 (2014) 2434–2439. https://doi.org/10.1016/j.joms.2014.08.012.

[3] T. Yoda, N. Ogi, H. Yoshitake, T. Kawakami, R. Takagi, K. Murakami, H. Yuasa, T. Kondoh, K. Tei, K. Kurita, Clinical guidelines for total temporomandibular joint replacement, Jpn. Dent. Sci. Rev. 56 (2020) 77–83. https://doi.org/10.1016/j.jdsr.2020.03.001.

[4] J. Durham, T.R.O. Newton-John, J.M. Zakrzewska, Temporomandibular disorders, BMJ 350 (2015) 1–9. https://doi.org/10.1136/bmj.h1154.

[5] S. Kanatsios, O. Breik, G. Dimitroulis, Biomet stock temporomandibular joint prosthesis: Long-term outcomes of the use of titanium condyles secured with four or five condylar fixation screws, J. Cranio-Maxillofacial Surg. 46 (2018) 1697–1702. https://doi.org/10.1016/j.jcms.2018.07.002.

[6] H.E. Giannakopoulos, D.P. Sinn, P.D. Quinn, Biomet microfixation temporomandibular joint replacement system: A 3-year follow-up study of patients treated during 1995 to 2005, J. Oral Maxillofac. Surg. 70 (2012) 787–794. https://doi.org/10.1016/j.joms.2011.09.031.

[7] S. Kerwell, M. Alfaro, R. Pourzal, H.J. Lundberg, Y. Liao, C. Sukotjo, L.G. Mercuri, M.T. Mathew, Examination of failed retrieved temporomandibular joint (TMJ) implants, Acta Biomater. 32 (2016) 324–335.

https://doi.org/10.1016/j.actbio.2016.01.001.

[8] J.N.A.R. Ferreira, C.C. Ko, S. Myers, J. Swift, J.R. Fricton, Evaluation of Surgically Retrieved Temporomandibular Joint Alloplastic Implants: Pilot Study, J. Oral Maxillofac. Surg. 66 (2008) 1112–1124. https://doi.org/10.1016/j.joms.2007.09.013.

[9] L.G. Mercuri, Temporomandibular joint replacement devices - dark past to challenging future, Stomatol. Dis. Sci. 2019 (2019). https://doi.org/10.20517/2573-0002.2018.25.

[10] J. Zhao, L. Zou, D. He, E. Ellis, Comparison of bone adaptation after modification in biomet standard alloplastic temporomandibular joint prostheses, J. Cranio-Maxillofacial Surg. 46 (2018) 1707–1711. https://doi.org/10.1016/j.jcms.2018.07.024.

[11] L.G. Mercuri, Alloplastic temporomandibular joint replacement: Rationale for the use of custom devices, Int. J. Oral Maxillofac. Surg. 41 (2012) 1033–1040. https://doi.org/10.1016/j.ijom.2012.05.032.

[12] L.M. Wolford, M.C. Pitta, O. Reiche-Fischel, P.F. Franco, TMJ concepts/techmedia custom-made TMJ total joint prosthesis: 5-year follow-up study, Int. J. Oral Maxillofac. Surg. 32 (2003) 268–274. https://doi.org/10.1054/ijom.2002.0350.

[13] L. Zou, D. He, E. Ellis, A Comparison of Clinical Follow-Up of Different Total Temporomandibular Joint Replacement Prostheses: A Systematic Review and Meta-Analysis, J. Oral Maxillofac. Surg. 76 (2018) 294–303. https://doi.org/10.1016/j.joms.2017.08.022.

[14] T.W.P. Korioth, D.P. Romilly, A.G. Hannam, Three□dimensional finite element stress analysis of the dentate human mandible, Am. J. Phys. Anthropol. 88 (1992) 69–96. https://doi.org/10.1002/ajpa.1330880107.

[15] T.W. Korioth, A.G. Hannam, Mandibular forces during simulated tooth clenching., J.

Orofac. Pain 8 (1994) 178–189. https://doi.org/https://pgocclusion.com/files/KoriothHannam01.pdf.

[16] I. Ichim, M. V. Swain, J.A. Kieser, Mandibular stiffness in humans: Numerical predictions, J. Biomech. 39 (2006) 1903–1913. https://doi.org/10.1016/j.jbiomech.2005.05.022.

[17] F. Gröning, M.J. Fagan, P. O'Higgins, The effects of the periodontal ligament on mandibular stiffness: A study combining finite element analysis and geometric morphometrics, J. Biomech. 44 (2011) 1304–1312. https://doi.org/10.1016/j.jbiomech.2011.01.008.

[18] F. Gröning, M. Fagan, P. O'higgins, Comparing the Distribution of Strains with the Distribution of Bone Tissue in a Human Mandible: A Finite Element Study, Anat. Rec. 296 (2013) 9–18. https://doi.org/10.1002/ar.22597.

[19] A.H. Choi, B. Ben-Nissan, R.C. Conway, Three-dimensional modelling and finite element analysis of the human mandible during clenching, Aust. Dent. J. 50 (2005) 42–48. https://doi.org/10.1111/j.1834-7819.2005.tb00084.x.

[20] R.T. Hart, V. V. Hennebel, N. Thongpreda, W.C. Van Buskirk, R.C. Anderson, Modeling the biomechanics of the mandible: A three-dimensional finite element study, J. Biomech. 25 (1992) 261–286. https://doi.org/10.1016/0021-9290(92)90025-V.

[21] A. Dutta, K. Mukherjee, V.S. Seesala, K. Dutta, R.R. Paul, S. Dhara, S. Gupta, Comparative evaluation of a patient-specific customised plate designs and screws for partial mandibular reconstruction, Med. Eng. Phys. 111 (2023) 103941. https://doi.org/10.1016/j.medengphy.2022.103941.

[22] A. Kashi, A.R. Chowdhury, S. Saha, Finite element analysis of a TMJ implant, J. Dent.

Res. 89 (2010) 241–245. https://doi.org/10.1177/0022034509357716.

[23] J. Huo, P. Dérand, L.E. Rännar, J.M. Hirsch, E.K. Gamstedt, Failure location prediction by finite element analysis for an additive manufactured mandible implant, Med. Eng. Phys. 37 (2015) 862–869. https://doi.org/10.1016/j.medengphy.2015.06.001.

[24] M. Mesnard, A. Ramos, Experimental and numerical predictions of Biomet® alloplastic implant in a cadaveric mandibular ramus, J. Cranio-Maxillofacial Surg. 44 (2016) 608–615. https://doi.org/10.1016/j.jcms.2016.02.004.

[25] B. Bekcioglu, E. Bulut, B. Bas, The Effects of Unilateral Alloplastic Temporomandibular Joint Replacement on the Opposite-Side Natural Joint: A Finite-Element Analysis, J. Oral Maxillofac. Surg. 75 (2017) 2316–2322. https://doi.org/10.1016/j.joms.2017.05.017.

[26] M. Pinheiro, R. Willaert, A. Khan, A. Krairi, W. Van Paepegem, Biomechanical evaluation of the human mandible after temporomandibular joint replacement under different biting conditions, Sci. Rep. 11 (2021) 1–12. https://doi.org/10.1038/s41598-021-93564-3.

[27] S.M. Ingawale, T. Goswami, Design and Finite Element Analysis of Patient-Specific Total Temporomandibular Joint Implants, Materials (Basel). 15 (2022). https://doi.org/10.3390/ma15124342.

[28] A. Gupta, A. Dutta, K. Dutta, K. Mukherjee, Biomechanical influence of plate configurations on mandible subcondylar fracture fixation: a finite element study, Med. Biol. Eng. Comput. 61 (2023) 2581–2591. https://doi.org/10.1007/s11517-023-02854-7.

[29] P. Ruf, V. Orassi, H. Fischer, C. Steffen, K. Kreutzer, G.N. Duda, M. Heiland, S. Checa, C. Rendenbach, Biomechanical evaluation of CAD/CAM magnesium miniplates as a fixation strategy for the treatment of segmental mandibular reconstruction with a fibula free flap, Comput. Biol. Med. 168 (2024) 107817. https://doi.org/10.1016/j.compbiomed.2023.107817.

[30] K. Mukherjee, S. Gupta, Bone ingrowth around porous-coated acetabular implant: a three-dimensional finite element study using mechanoregulatory algorithm, Biomech. Model. Mechanobiol. 15 (2016) 389–403. https://doi.org/10.1007/s10237-015-0696-7.

[31] R. Ghosh, S. Chanda, D. Chakraborty, Qualitative predictions of bone growth over optimally designed macro-textured implant surfaces obtained using NN-GA based machine learning framework, Med. Eng. Phys. 95 (2021) 64–75. https://doi.org/10.1016/j.medengphy.2021.08.002.

[32] BIOMET Microfixation, Mandibular Joint Replacement System by Zimmer Biomet, 2007. https://doi.org/http://www.wlorenz.com.co/sites/default/files/documentos_producto/TMJ.pdf.

[33] L. Hijazi, W. Hejazi, M.A. Darwich, K. Darwich, Finite element analysis of stress distribution on the mandible and condylar fracture osteosynthesis during various clenching tasks, Oral Maxillofac. Surg. 20 (2016) 359–367. https://doi.org/10.1007/s10006-016-0573-2.

[34] R. Fan, J. Liu, Z. Jia, Biomechanical evaluation of different strain judging criteria on the prediction precision of cortical bone fracture simulation under compression, Front. Bioeng. Biotechnol. 11 (2023) 1–9. https://doi.org/10.3389/fbioe.2023.1168783.

[35] E. Schileo, E. Dall'Ara, F. Taddei, A. Malandrino, T. Schotkamp, M. Baleani, M.

Viceconti, An accurate estimation of bone density improves the accuracy of subject-specific finite element models, J. Biomech. 41 (2008) 2483–2491. https://doi.org/10.1016/j.jbiomech.2008.05.017.

[36] C. Meyer, J.L. Kahn, P. Boutemi, A. Wilk, Photoelastic analysis of bone deformation in the region of the mandibular condyle during mastication, J. Cranio-Maxillofacial Surg. 30 (2002) 160–169. https://doi.org/10.1054/jcms.2002.0297.

[37] M.U. Farooq, M.P. Mughal, N. Ahmed, N.A. Mufti, A.M. Al-Ahmari, Y. He, On the investigation of surface integrity of Ti6Al4V ELI using si-mixed electric discharge machining, Materials (Basel). 13 (2020). https://doi.org/10.3390/ma13071549.

[38] L.E. Claes, C.A. Heigele, Magnitudes of local stress and strain along bony surfaces predict the course and type of fracture healing, J. Biomech. 32 (1999) 255–266. https://doi.org/10.1016/S0021-9290(98)00153-5.

[39] D.R. Carter, G.S. Beaupré, N.J. Giori, J.A. Helms, Mechanobiology of Skeletal Regeneration, Clin. Orthop. Relat. Res. 355 (1998). https://doi.org/https://journals.lww.com/clinorthop/fulltext/1998/10001/mechanobiology_of_skeletal_regeneration.6.aspx.

[40] J.-P. van Loon, L.G.M. de Bont, F.K.L. Spijkervet, G.J. Verkerke, R.S.B. Liem, A short-term study in sheep with the Groningen temporomandibular joint prosthesis, Int. J. Oral Maxillofac. Surg. 29 (2000) 315–324. https://doi.org/10.1034/j.1399-0020.2000.290501.x.

[41] T. Sugiura, K. Horiuchi, M. Sugimura, S. Tsutsumi, Evaluation of threshold stress for bone resorption around screws based on in vivo strain measurement of miniplate., J. Musculoskelet. Neuronal Interact. 1 (2000) 165–70. http://www.ncbi.nlm.nih.gov/pubmed/15758514.

[42] M.R. Niroomand, M. Arabbeiki, Implant stability in different implantation stages: Analysis of various interface conditions, Informatics Med. Unlocked 19 (2020) 100317. https://doi.org/10.1016/j.imu.2020.100317.

[43] R. Ghosh, S. Chanda, D. Chakraborty, The influence of macro-textural designs over implant surface on bone on-growth: A computational mechanobiology based study, Comput. Biol. Med. 124 (2020) 103937. https://doi.org/10.1016/j.compbiomed.2020.103937.

[44] J.A. Inzana, P. Varga, M. Windolf, Implicit modeling of screw threads for efficient finite element analysis of complex bone-implant systems, J. Biomech. 49 (2016) 1836–1844. https://doi.org/10.1016/j.jbiomech.2016.04.021.

Figures

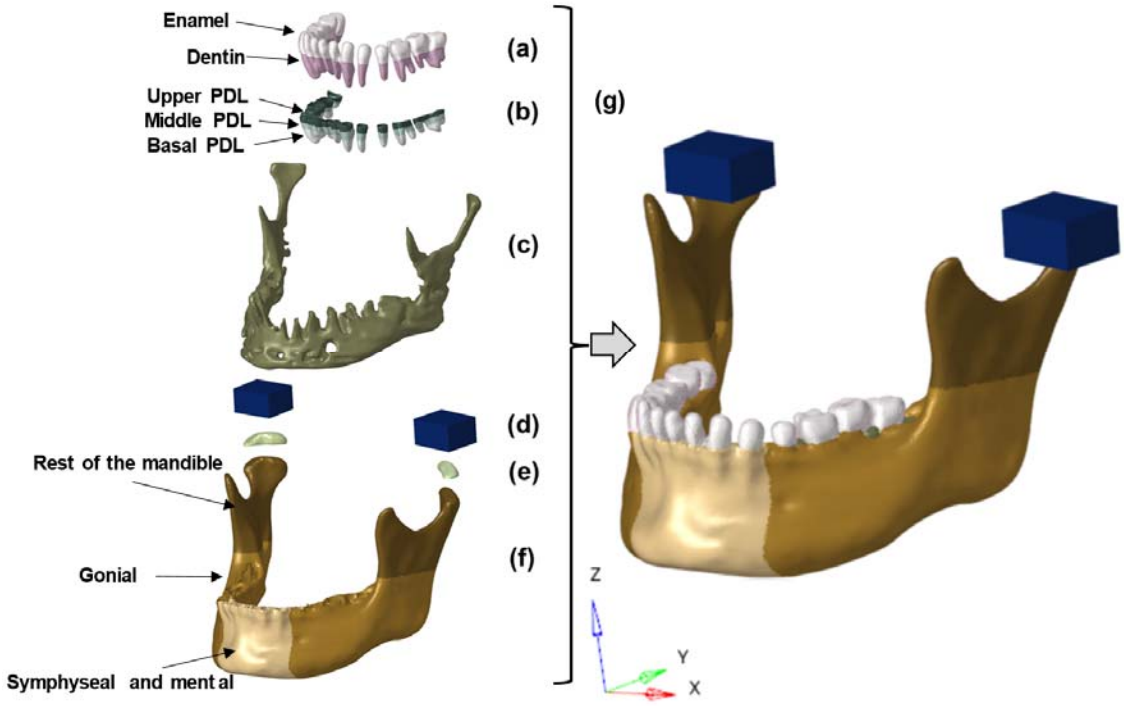

Figure 1 Different components of the developed mandible model: (a) teeth with enamel and dentin; (b) periodontal ligament (PDL) comprising of upper, middle, and basal PDL; (c) cancellous bone; (d) blocks representing temporal bone; (e) articular fibrocartilage; (f) cortical bone with three major regions: symphyseal and mental, gonial, rest of the mandible; and (g) the complete mandible model.

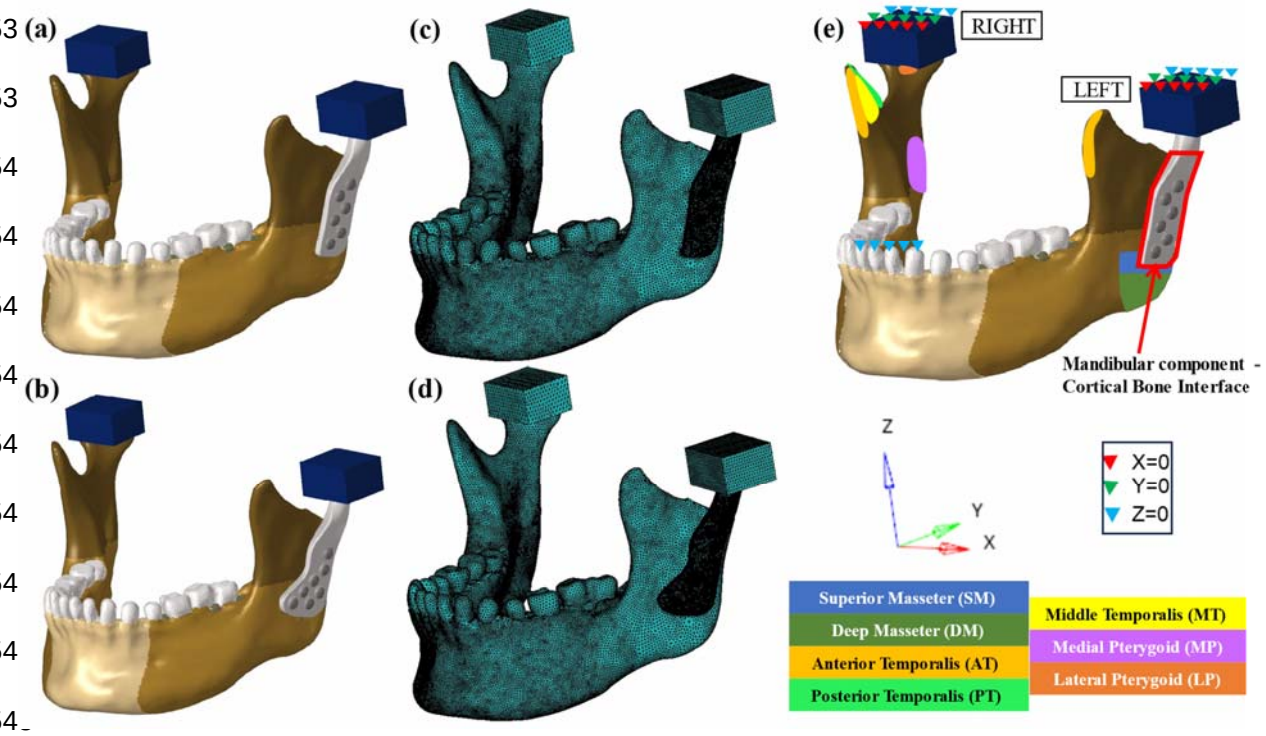

Figure 2 Developed FE models of implanted mandibles: (a, c) Narrow TMJ Implant (b, d) Standard TMJ Implant (e) muscle attachment sites and representative boundary conditions for incisor (INC) loading condition.

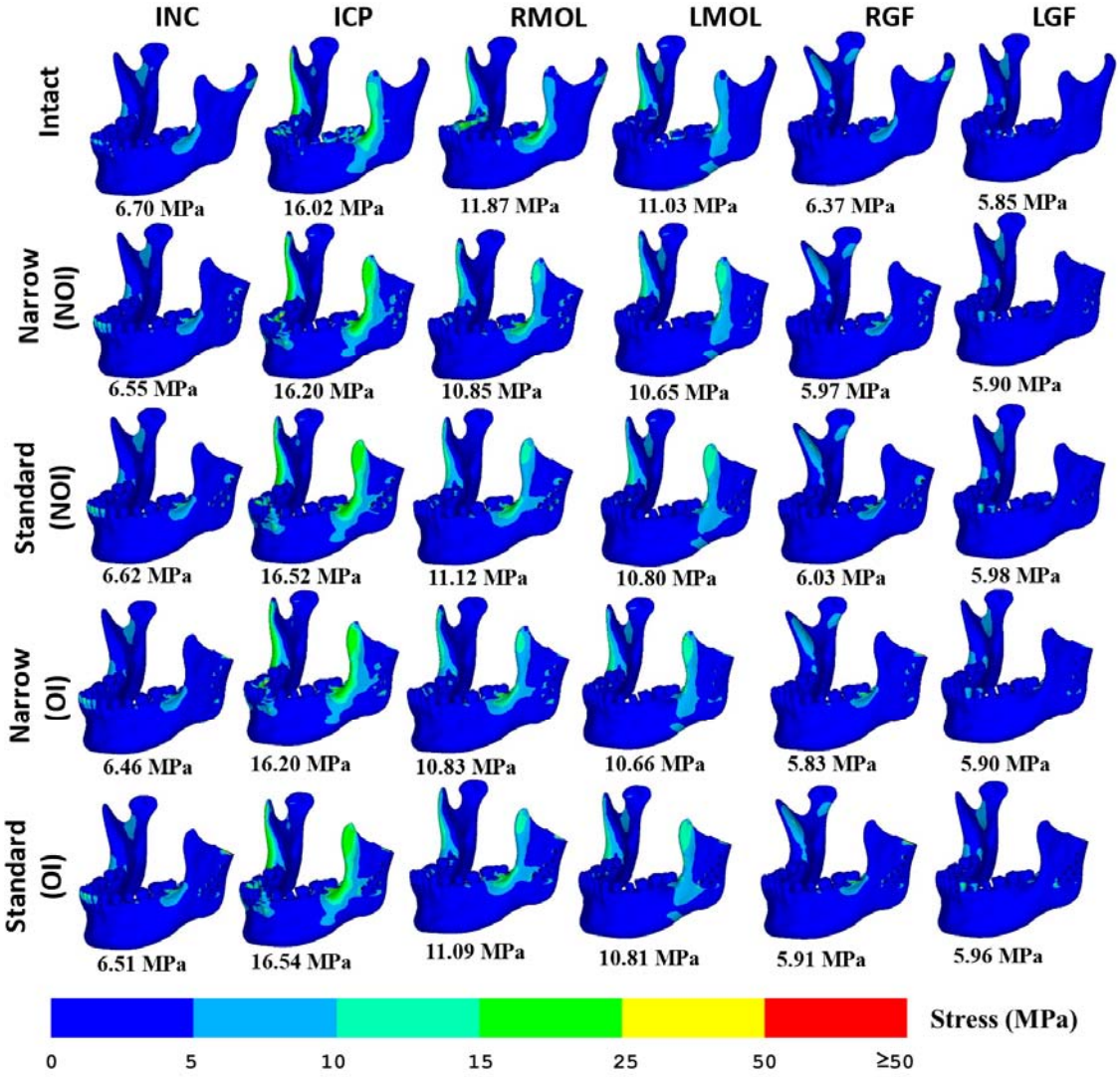

Figure 3 Maximum principal stress distributions across intact and implanted mandibles under complete mastication cycle. For implanted mandibles, stress distributions for both non-osseointegrated (NOI) and osseointegrated (OI) conditions are shown.

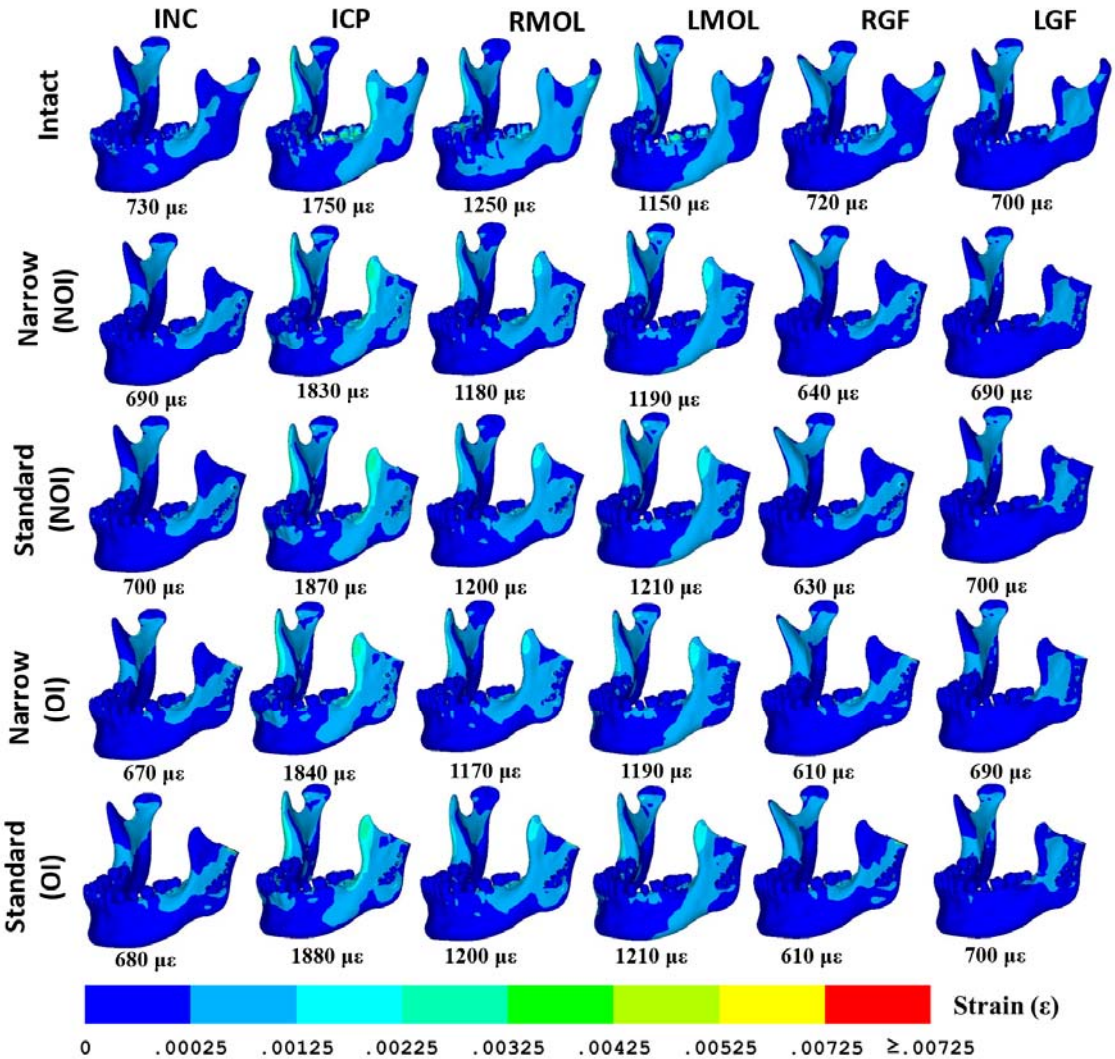

Figure 4 Maximum principal strain distribution across the intact and implanted mandibles under complete mastication cycle. For implanted mandible, strain distributions during both non-osseointegrated (NOI) and osseointegrated (OI) conditions are shown.

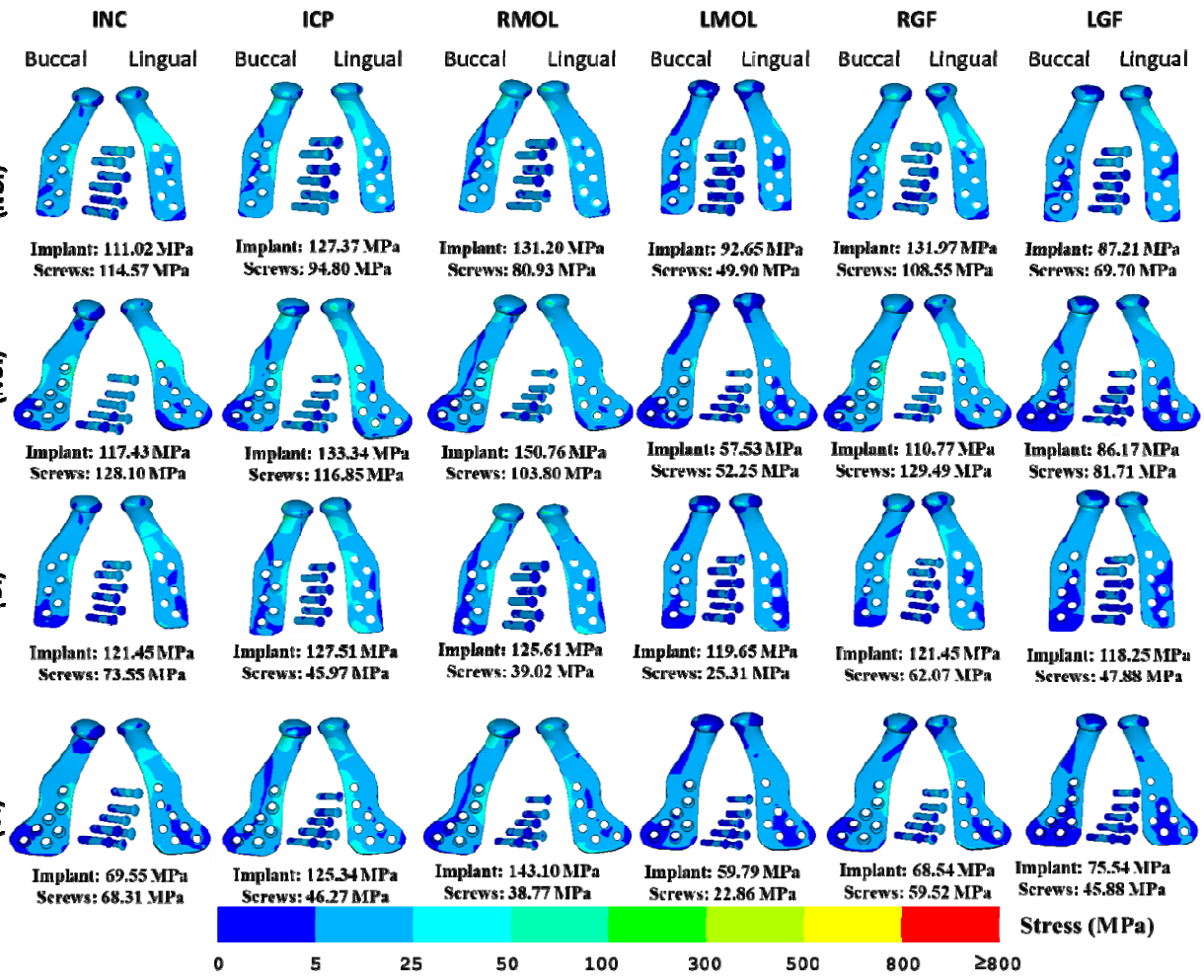

Figure 5 von Mises stress distribution in narrow and standard TMJ implants and screws under complete mastication cycle during non-osseointegrated (NOI) and osseointegrated (OI) conditions.

Tables

Table 1: Material properties of the components of the FE model [14]

Components	Young's Modulus (GPa)			Poisson's Ratio			Shear Modulus (GPa)		
	E_x	E_y	E_z	ν_{xy}	ν_{yz}	ν_{xz}	G_{xy}	G_{yz}	G_{xz}
Cortical									
Symphyseal and mental	23	10	15	0.3	0.3	0.3	4.8	3.6	6.2
Gonial angle region	20	11	12	0.3	0.3	0.3	4.8	5.3	6.0
Rest of the cortical	17	6.9	8.2	0.3	0.3	0.3	2.8	2.9	4.6
Cancellous	0.96	0.32	0.39	0.3	0.3	0.3	0.09	0.13	0.17
Enamel	80	-	-	0.3	-	-	-	-	-
Dentin	17.6	-	-	0.25	-	-	-	-	-
Periodontal ligament									
Coronal third	0.0032	-	-	0.45	-	-	-	-	-
Middle third	0.0027	-	-	0.45	-	-	-	-	-
Apical third	0.0025	-	-	0.45	-	-	-	-	-
Fibrocartilage	0.006	-	-	0.47	-	-	-	-	-
Mandibular component and Screws (Ti-6Al-4V ELI)	113.8	-	-	0.342	-	-	-	-	-

Table 2: Muscle forces and boundary conditions simulating different clenching activities [21,33]

Clenching tasks	**Side**	**Direction**	**Muscular force (N)**							**Boundary Condition**
			SM	**DM**	**MP**	**AT**	**MT**	**PT**	**LP**	
INC	Right	Force	76.2	21.2	136.4	12.6	5.7	3.0	47.5	Constrained the incisor regions
		F_x	−15.8	−11.6	66.3	−1.9	−1.3	−0.6	29.9	
		F_y	−31.9	7.6	−50.9	−0.6	2.9	2.6	−36.0	
		F_z	67.3	16.1	107.8	12.5	4.8	1.4	−8.3	
	Left	Force	76.2	21.2	136.4	12.6	5.7	3.0	47.5	
		F_x	15.8	11.6	−66.3	1.9	1.3	0.6	−29.9	
		F_y	−31.9	7.6	−50.9	−0.6	2.9	2.6	−36.0	
		F_z	67.3	16.1	107.8	12.5	4.8	1.4	−8.3	
ICP	Right	Force	190.4	81.6	132.9	154.9	91.8	71.0	18.1	Constrained the canine and premolars
		F_x	−39.4	−44.6	64.6	−23.1	−20.4	−14.8	11.4	
		F_y	−79.80	29.2	−49.61	−6.8	45.9	60.8	−13.7	
		F_z	168.3	61.9	105.1	153.0	76.8	33.7	−3.1	
	Left	Force	190.4	81.6	132.9	154.9	91.8	71.0	18.1	
		F_x	39.4	44.6	−64.6	23.1	20.4	14.8	−11.4	
		F_y	−79.8	29.2	−49.6	−6.8	45.9	60.8	−13.7	
		F_z	168.3	61.9	105.1	153.0	76.8	33.7	−3.1	
RMOL	Right	Force	137.1	58.8	146.9	115.4	63.1	44.6	20.1	Constrained the right molars
		F_x	−28.4	−32.1	71.4	−17.2	−14.0	−9.3	12.6	
		F_y	−57.4	21.0	−54.8	−5.1	31.5	38.1	−15.2	
		F_z	121.2	44.5	116.1	114.0	52.8	21.1	−3.5	
	Left	Force	114.2	49.0	104.9	91.7	64.0	29.5	43.5	
		F_x	23.6	26.7	−51.0	13.7	14.2	6.1	−27.4	

		F_y	−47.9	17.5	−39.1	−4.0	32.0	25.2	−32.9	
		F_z	101.0	37.1	83.0	90.5	53.6	14.0	−7.6	
LMOL	Right	Force	114.2	49.0	104.9	91.7	64.0	29.5	43.5	Constrained the left molars
		F_x	−23.6	−26.7	51.0	−13.7	−14.2	−6.1	27.4	
		F_y	−47.9	17.5	−39.1	−4.0	32.0	25.2	−32.9	
		F_z	101.0	37.1	83.0	90.5	53.6	14.0	−7.6	
	Left	Force	137.1	58.8	146.9	115.4	63.1	44.6	20.1	
		F_x	28.4	32.1	−71.4	17.2	14.0	9.3	−12.6	
		F_y	−57.4	21.0	−54.8	−5.1	31.5	38.1	−15.2	
		F_z	121.2	44.5	116.1	114.0	52.8	21.1	−3.5	
RGF	Right	Force	34.3	29.4	12.2	104.3	61.2	46.8	39.5	Constrained the right canine, premolars and molars
		F_x	−7.1	−16.0	5.9	−15.5	−13.6	−9.7	24.9	
		F_y	−21.5	7.6	−49.6	−0.5	2.9	3.9	−7.1	
		F_z	45.4	16.1	105.1	10.9	4.8	2.2	−1.6	
	Left	Force	51.4	21.2	132.9	11.1	5.7	4.5	9.4	
		F_x	10.6	11.6	−64.6	1.6	1.3	0.9	−5.9	
		F_y	−21.5	7.6	−49.6	−0.5	2.9	3.9	−7.1	
		F_z	45.4	16.1	105.1	10.9	4.8	2.2	−1.6	
LGF	Right	Force	51.4	21.2	132.9	11.1	5.7	4.5	9.4	Constrained the left canine, premolars and molars
		F_x	−10.6	−11.6	64.6	−1.6	−1.3	−0.9	5.9	
		F_y	−21.5	7.6	−49.6	−0.5	2.9	3.9	−7.1	
		F_z	45.4	16.1	105.1	10.9	4.8	2.2	−1.6	
	Left	Force	34.3	29.4	12.2	104.3	61.2	46.8	39.5	
		F_x	7.1	16.0	−5.9	15.5	13.6	9.7	−24.9	
		F_y	−21.5	7.6	−49.6	−0.5	2.9	3.9	−7.1	
		F_z	45.4	16.1	105.1	10.9	4.8	2.2	−1.6	